ELSEVIER

Physica A 240 (1997) 419–431

PHYSICA A

Formation, growth and precipitation of fractal molecular aggregates in porous media

Muhammad Sahimi, Hossein Rassamdana

Department of Chemical Engineering, University of Southern California, Los Angeles, CA 90089-1211, USA

Received 5 December 1996

Abstract

Analysis of small-angle scattering data, as well as novel precipitation measurements, are used to delineate the structure of the molecular aggregates that are formed when a fluid is injected into a porous medium to displace the in-place fluid. Our analysis suggests conclusively that these aggregates are fractal formed by diffusion-limited processes. The implications for the molecular weight distribution of the aggregates and modelling their flow and precipitation in a porous medium are discussed.

1. Introduction

Formation, flow and precipitation of large particles or aggregates in porous media is relevant to a wide variety of natural and industrial processes, and has been studied for a long time [1]. Examples include deep-bed filtration [2–4], ground water contamination [5], flow of dilute stable emulsions [6,7], migration of electrically charged colloidal particles [2,8], catalysis [8,9], and enhanced oil recovery [10,11]. The efficiency of these processes depends crucially on the availability of open pore space for flow of the fluid that carries the aggregates. In some cases, the aggregates are formed when the fluid in the porous medium reacts with the solid matrix, resulting in solid products that are carried away by the flowing fluid. In other cases, they are formed (see below) when a fluid is injected into the pore space to react with, or displace, the in-place fluid; it is this case that is the focus of this paper. These aggregates have very unusual properties, and have even been used [12] for manufacturing strong composite materials that have many industrial applications. Depending on the system in which they are formed, or their application, they are also called with a variety of names. For example, in enhanced oil recovery and catalytic processes they are referred to as *asphalts*. Despite many years of research, a definitive model of such aggregates has not emerged, and

PII S0378-4371(97)00034-4

thus the dependence of their structure on the composition of the fluids, the temperature and pressure of the system, and the type of the solvent that is used for their formation cannot be predicted.

Consider a typical process in which such aggregates are formed, e.g., enhanced recovery of oil from underground reservoirs. In this process, an agent or solvent, a gas or a liquid, is injected into the reservoir to displace the in-place oil. The oil contains very small colloidal particles (or micelles) whose surface is covered by protective materials such as resin, which prevent their aggregation. The solvent dissolves the protective materials, and since the colloidal particles are charged, the dissolution of their protective materials frees them to join each other upon collision with one another in the solution. This causes the formation and precipitation of the large molecular aggregates. A similar phenomenon occurs in many catalytic processes involving a porous catalyst when a reactant penetrates its pore space. Moreover, ground waters in aquifers often contain solid, electrically charged particles that are covered by some minerals. When a reactive pollutant is introduced into an aquifer, it dissolves the surface minerals and allows the charged particles to aggregate together. Typical size of these aggregates is usually much smaller than the typical pore sizes in a sandstone [13] which vary between 10 and 90 μm, so that the presence of the pore walls does not normally hinder formation of such aggregates. Outside a porous medium, under bulk conditions, aggregates of this kind can form and they are much larger than those grown in the medium. However, the properties of such aggregates are usually similar [14] to those that are formed in the porous medium. In this paper we analyze accurate small-angle scattering data, as well as novel precipitation measurements, to show that these aggregates are fractal with structures similar to diffusion-limited aggregation (DLA) clusters [15] and diffusion-limited cluster–cluster (DLCC) aggregates [16,17]. This has important implications which are discussed below.

The plan of this paper is as follows. In the next section we present an analysis of small-angle scattering data, and study the effect of a variety of factors, such as the temperature and pressure of the system. We then present the precipitation data and provide a scaling analysis of them. Next, the connection between the two types of aggregates is discussed, and a scaling relation linking the two is derived. The paper is summarized and discussed in the last section.

2. Small-angle scattering

An accurate method for investigating the structure of these aggregates is to form them in a tube or cell by mixing the in-place fluid, e.g., a crude oil, with a solvent and studying the resulting aggregates by small-angle X-ray and neutron scattering (SAXS and SANS, respectively). As we suggest below, a novel method for studying these aggregates is based on precipitation experiments. In a scattering experiment the observed scattering intensity $I_s(\mathbf{q})$ by a single aggregate is given by the Fourier transform of the

correlation function $C(\mathbf{r})$

$$I_s(\mathbf{q}) = \int_0^\infty C(\mathbf{r}) \exp(i\mathbf{q} \cdot \mathbf{r}) d^3\mathbf{r} \,. \tag{1}$$

Normally, the solution contains many aggregates of various sizes. We assume that $n_s(t)$ is the number of aggregates of size s at time t, where s refers to the number of the elementary particles in an aggregate. Then the total scattering intensity $I(q)$ ($q = |\mathbf{q}|$) by all the aggregates is [18]

$$I(q) = \int s n_s I_s(q) ds \,. \tag{2}$$

We assume a power-law distribution [19]

$$n_s(t) \sim s^{-\tau} f(s/\langle s \rangle) \,, \tag{3}$$

where $\langle s \rangle \sim t^w$ is the mean aggregate size, and $f(x)$ is a universal scaling function such that $f(x) \sim x^\delta$ for $x \ll 1$, and $f(x) \ll 1$ for $x \gg 1$. For fractal aggregates in d dimensions, $C(r) \sim r^{D_f - d}$ ($r = |\mathbf{r}|$), where D_f is the fractal dimension of the aggregates, and thus

$$I(q) \sim q^{-(3-\tau)D_f} \,. \tag{4}$$

We point out that the exact form of $I(q)$ is more complex than Eq. (4), but for discussing the scaling properties of the aggregates Eq. (4) suffices. Later in this paper we discuss fitting of the scattering data to a more elaborate equation. Eq. (4) predicts that a logarithmic plot of $I(q)$ versus q should yield a straight line with a slope $p = -(3 - \tau)D_f$.

The scattering intensity $I(q)$ versus q in a typical SANS experiment [20] is shown in Fig. 1, where n-C_7 was the solvent. In these experiments the wavelength was 5.0 Å, and the sample-to-detector distance was 180 cm, which corresponds to a q-range of 0.008 to 0.17 Å. The injected fluid was n-C_7, and after the aggregates were formed they were separated from the solution and mixed with toluene. The scattering experiments were carried out after 11 d. As can be seen, there are two distinct regimes described by two distinct fractal dimensions d_f and D_f, corresponding to small and large aggregates (length scales). At large (small) length scales (q), one obtains a straight line with a slope of about -1.75 ± 0.05, whereas at small (large) length scales (q) the slope is about -2.5 ± 0.1. To interpret these results we resort to our experimental observations, which indicate the following mechanisms for the formation of the aggregates. After the solvent is added and the protective materials are partially removed from the surface of the elementary charged colloidal particles, they diffuse in the solution and stick to one another upon collision. At short times only small clusters that are the result of particle aggregation are formed. Thus, the small aggregates should have the structure of DLA clusters, which in 3D have a fractal dimension of about $d_f \simeq 2.5$, in agreement with the results shown in Fig. 1 for large qs. The extent of particle aggregation depends

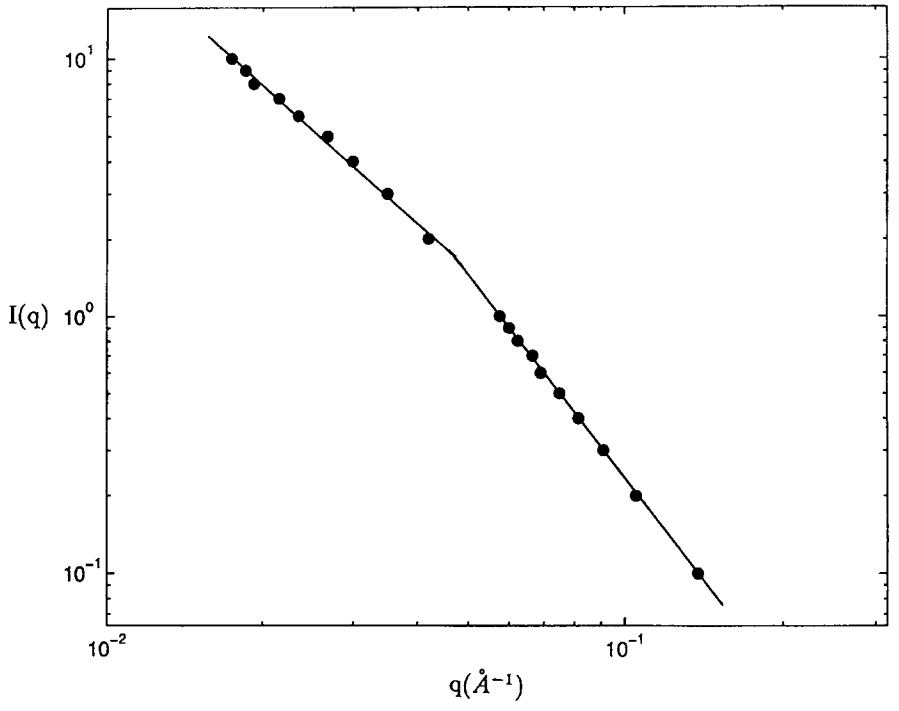

Fig. 1. The scattering intensity $I(q)$ versus q at $T = 25°C$. Symbols are the data, and the straight lines represent their best fit.

on the amount of the solvent injected into the system, and the fraction of the particles whose surface has been "cleaned" by the solvent. After some time, the solution contains a mixture of small aggregates and possibly individual colloidal particles, all of which continue to diffuse in the solution. The small aggregates, whose surface are also charged, stick to one another upon collision to form larger aggregates. Therefore, at large length scales the aggregates should have the structure of 3D DLCC aggregates for which $\tau = 2$ and $D_f \simeq 1.75$, so that the slope of the straight line must be about -1.75, again in perfect agreement with the results shown in Fig. 1. Precipitation starts only when the weight of the aggregates is large enough; this is discussed below.

We should point out that Eq. (4) provides a self-consistency check of the interpretation of the scattering results. That is, since for every universality class of fractal structures there are distinct values of τ and D_f, the combination $-(3 - \tau)D_f$ for a given universality class must be consistent with the slope of the scattering curve. For example, suppose that the aggregates in the solution had been formed by a percolation process (although there is no physical justification for this). Since for percolation in 3D we have $\tau \simeq 2.18$ and $D_f \simeq 2.52$, the slope of the scattering curve (at large length scales) must be -2.07, which does not agree with -1.75 obtained from the data. In this sense, the DLCC aggregation provides the only plausible interpretation of the data.

3. The effect of temperature and pressure on the structure of the aggregates

In many practical applications, such as enhanced oil recovery or catalytic processes, the systems in which such aggregates are formed operate at high temperatures and pressures. Therefore, it is important to understand what happens to the structure of the aggregates under such conditions. As the temperature increases the rotational (as well as translational) motion of the particles and the small aggregates in the solution increases. It is known [21] that, if in DLCC aggregation the clusters are allowed to rotate, the fractal dimension of the final aggregate decreases from its value $D_f \simeq 1.75$ without rotation, reaching $D_f \simeq 1$ for fast rotations. Thus, at high temperatures we expect to have aggregates with $D_f \simeq 1.0$. Fig. 2 shows SAXS results [22] for a system at 80°C with n-C_{10} as the solvent, which indicates that $D_f \simeq 1$ at large length scales. Therefore, even at high temperatures, the formation mechanism of these clusters is DLCC aggregation accompanied by fast rotation of the smaller clusters that give rise to lower fractal dimensions.

The effect of pressure on the value of D_f is similar to that of the temperature, i.e., at high pressures the fractal dimension of the aggregates is lower than that at atmospheric pressure, although in this case the reason for the reduction in the fractal dimension is different from that of high temperatures. At a fixed temperature, a low pressure is

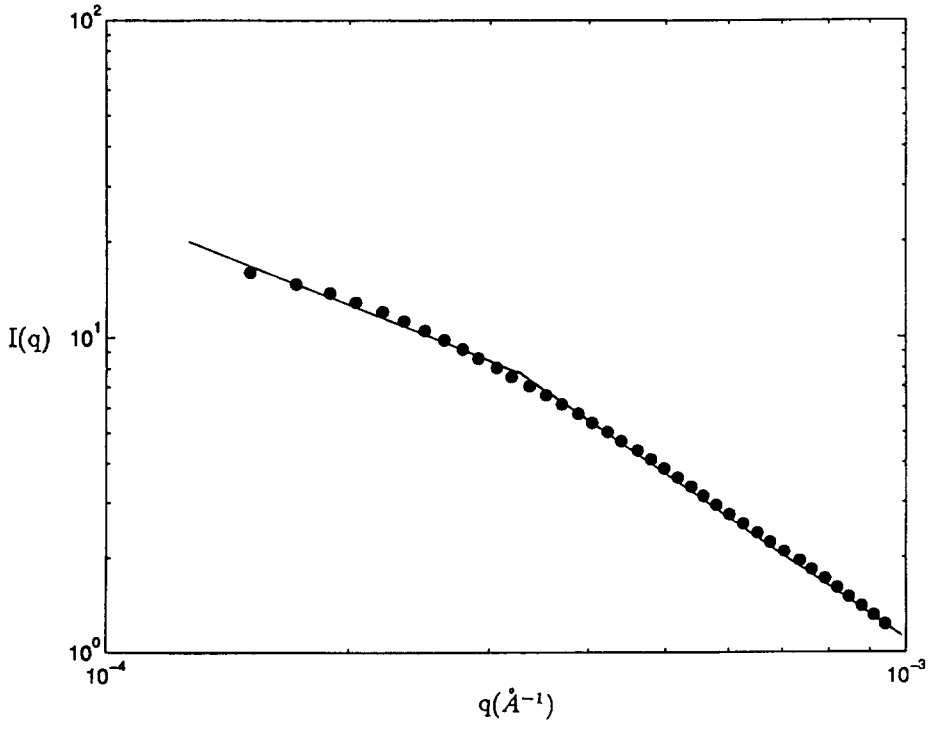

Fig. 2. The same as in Fig. 1, but at $T = 80°C$ and $P = 14.7$ psia.

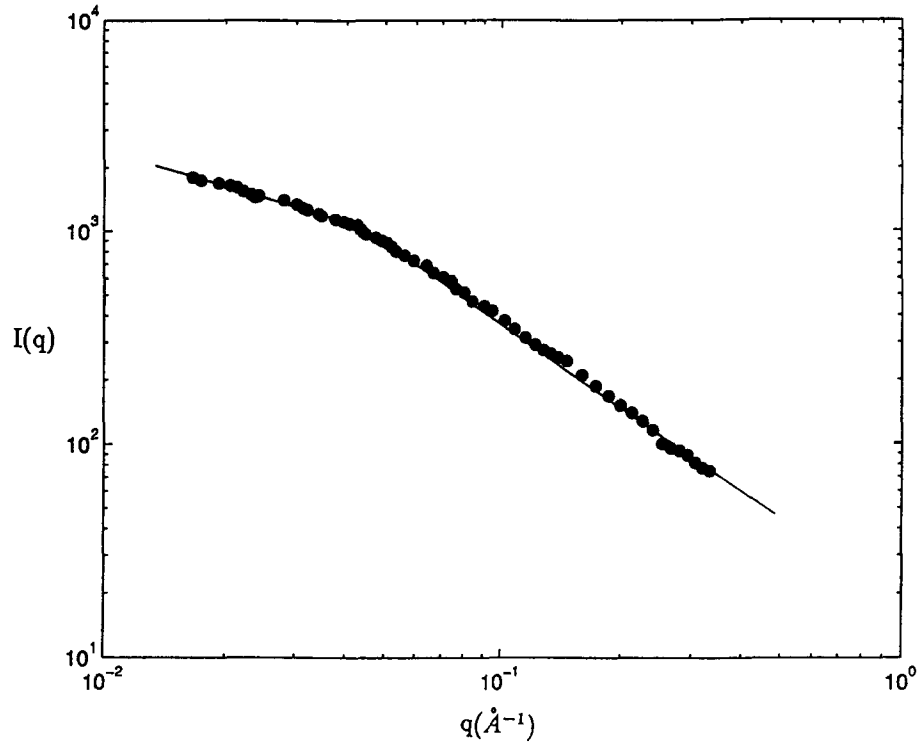

Fig. 3. The same as in Fig. 1, but at $T = 25°C$ and $P = 5900$ psia.

associated with lower solution densities and solubilizing ability, and a large mean distance between the aggregate particles and the surrounding fluid particles, resulting in $D_f \simeq 1.75$ and $d_f \simeq 2.5$. However, as the pressure increases the solubilizing ability of the solution increases, and thus smaller aggregates with much lower fractal dimensions should form. Fig. 3 shows SAXS results [23] at 25°C and $P = 5900$ psia, with n-C_5 as the solvent. At small length scales one has $d_f \simeq 1.3$, much smaller than $d_f \simeq 2.5$ which is the expected value for atmospheric pressures, while at large length scales one has $D_f \simeq 1.0$, in agreement with our arguments.

4. Precipitation measurements

We now consider the problem from a novel angle, namely, precipitation of the aggregates, and show that the *amount* of the precipitation also provides insights into their structure that are consistent with the scattering data. We have done experiments both in a tube and in a porous medium. The porous medium was a random packing of glass beads with equal diameters. Three different porous media, with three different bead sizes were used. However, as we mentioned above, usually the size of the aggregates is much smaller than the average pore size, and thus the results with the

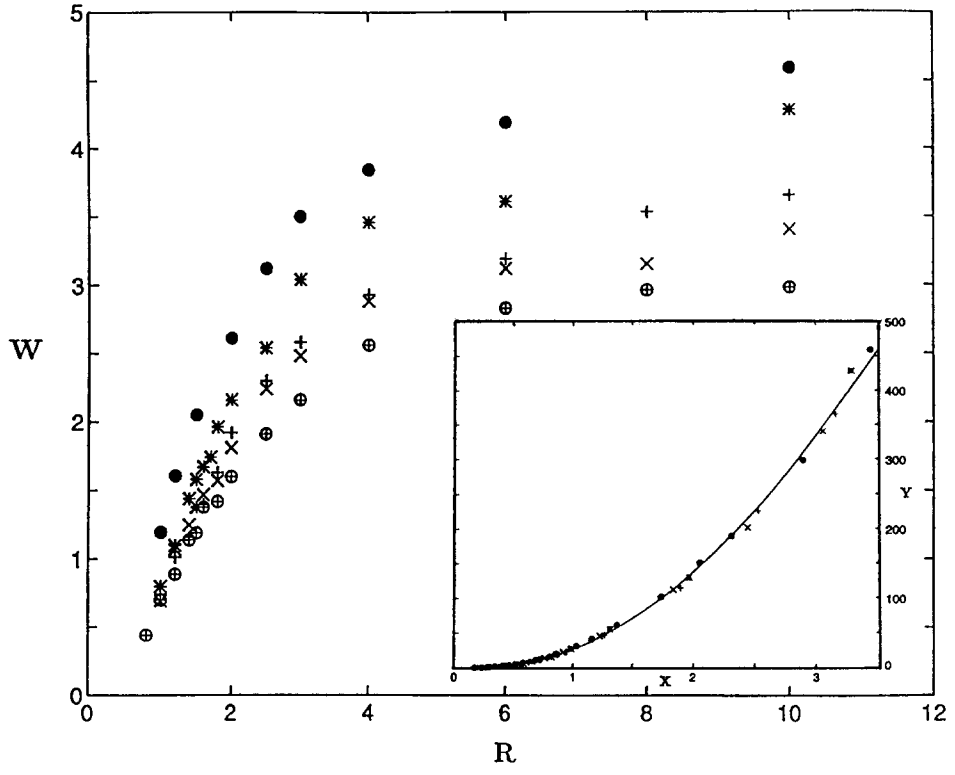

Fig. 4. The weight percent $W(t)$ of the precipitated aggregates versus the solvent to oil ratio R. The solvents are, from top to bottom, n-C_5, n-C_6, n-C_7, n-C_8, and n-C_{10}. The inset shows the data collapse with $X = R/M_s^{1/4}$ and $Y = WR^2$, where M_s is the MW of the solvent.

porous media were completely consistent with the tube results. To measure the amount of the precipitated aggregates we diluted a crude oil by a solvent, a n-alkane ranging from C_5 to C_{10}. Several different dilution ratios R, measured in terms of the cm^3 of the solvent/gr of the oil, were used. The diluted oil was then agitated in a tube at 25°C to complete mixing of the solvent with the oil. After one day the amount of the precipitated aggregates was measured. The results, in terms of the weight percent $W(t)$ of the aggregates, are presented in Fig. 4. Note that in general W is a function of the time t at which the measurements are done, since the aggregation process is a dynamic phenomenon. Fig. 4 suggests that one may collapse the data onto a single universal curve. The variables in Fig. 3 are R, W, and M_s, the molecular weight (MW) of the solvent. We find that with $X = R/M_s^z$ and $Y = R^{z'}W$ the data collapse onto a single curve with $z = 1/4$ and $z' = 2$; this is shown in the inset of Fig. 4. To understand this, note that for the DLCC aggregates one has [19] a dynamic scaling similar to Eq. (3) with $\tau = 2$, so that

$$s^2 n_s(t) = f(s/\langle s\rangle)\,. \tag{5}$$

The fact that $z' = 2$ means that our scaling curve is represented by $Y = h(X)$, and thus

$$R^2 W = h(R/M_s^z)\,, \tag{6}$$

which is similar to the dynamic scaling for the DLCC aggregates, Eq. (5). This implies that in the precipitation experiments the group $R^2 W(t)$ has a role similar to $s^2 n_s(t)$ in the DLCC experiments. Although it is tempting to assert that $W(t)$ is proportional to $n_s(t)$ (since obviously the amount of precipitation at time t should be related to the number of the aggregates at that time), strictly speaking this is not correct, because in general one expects to have

$$W(t) \sim \int_{s_{min}}^{s_{max}} s n_s(t) ds\,, \tag{7}$$

where s_{min} and s_{max} are the minimum and maximum size of the aggregates that precipitate. Eq. (7) is the mathematical statement of the fact that $W(t)$ is simply proportional to the total number of particles in all aggregates whose sizes are larger than a critical size s_{min}. If the aggregates are too small, $s < s_{min}$, they will remain suspended in the solution. We expect to have $s_{min} \sim \alpha \langle s \rangle$, where $\alpha > 1$. On the other hand, it is known [24] that fractal aggregates cannot become too large; once their size exceeds a critical size, they lose their mechanical stability and have to rearrange themselves. Thus, there is an upper bound s_{max} to the size of these aggregates, which also imposes an upper limit on the molecular weight of these aggregates. Note that, a comparison of Eqs. (5) and (6) also indicates that the mean aggregate size $\langle s \rangle$ is related to the molecular weight M_s of the solvent through $\langle s \rangle \sim M_s^z$.

Summarizing this section, precipitation measurements can be expressed in terms of a universal dynamic scaling similar to that for DLCC aggregates, but the details of the scalings in the two phenomena are not necessarily the same.

5. Connection between small-angle scattering and precipitation

The range of the length scales in the scattering data is not very large. Thus, one may be tempted to fit the entire curve to a single scattering function, rather than distinguishing between the structure of the aggregates at small and large length scales, as we have done here. Hence, in this section we derive an expression for the amount of the aggregates *remaining in the solution* (i.e., the total amount of the aggregates minus the precipitated amount) to show that, (1) one needs *two* fractal dimensions to describe the data, and thus our practice of distinguishing the small aggregates from the large ones is sound, and (2) simple precipitation measurements provide insight into the aggregates' structure. The volume of an aggregate of size s is $v \sim s^{3/D_f}$, and thus

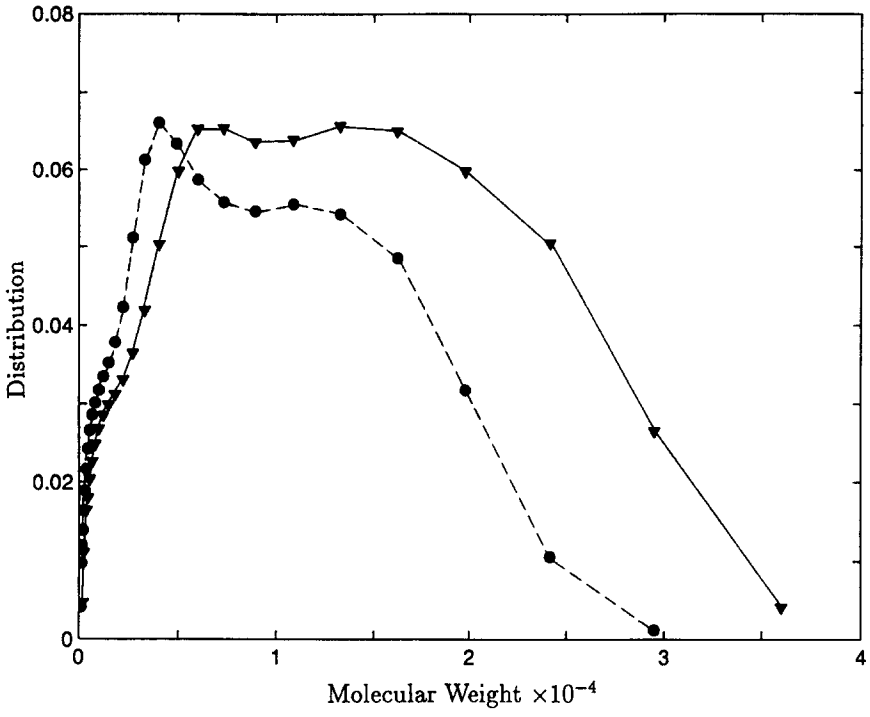

Fig. 5. The MW distribution of the aggregates with n-C_5 (•) and n-C_{10} (▼) as the solvent at $T = 25°C$.

the volume of all the aggregates remaining in the solution is

$$V(t) \sim \int_1^{s_{min}} v n_s(t) ds \,, \tag{8}$$

where s_{min} is the minimum size of an aggregate that can precipitate, and thus all aggregates whose sizes are smaller than s_{min} remain in the solution and do not precipitate. As discussed above, we expect to have $s_{min} \sim \alpha \langle s \rangle$, and thus

$$V(t) \sim \int_1^{s_{min}} s^{3/D_f} s^{-\tau} f(s/\langle s \rangle) ds = \langle s \rangle^{3/D_f - \tau + 1} \int_1^{\alpha} x^{3/D_f - \tau} f(x) dx \sim \langle s \rangle^{3/D_f - \tau + 1} \,. \tag{9}$$

The typical aggregate remaining in the solution has a volume v_t in terms of which $V(t) \sim v_t^{[3+D_f(1-\tau)]/3}$. In a solution that contains one or a few relatively large aggregates with a fractal dimension D_f and a large number of small aggregates with a fractal dimension d_f, the typical aggregate size is dominated by those of the small clusters. That is, the mean aggregate size *remaining in the solution* is dominated by the small aggregates (since if they are large enough, they would precipitate). Therefore, we can write $v_t \sim \ell^{d_f}$, where ℓ is the radius of the typical aggregate. If ρ is the density of the

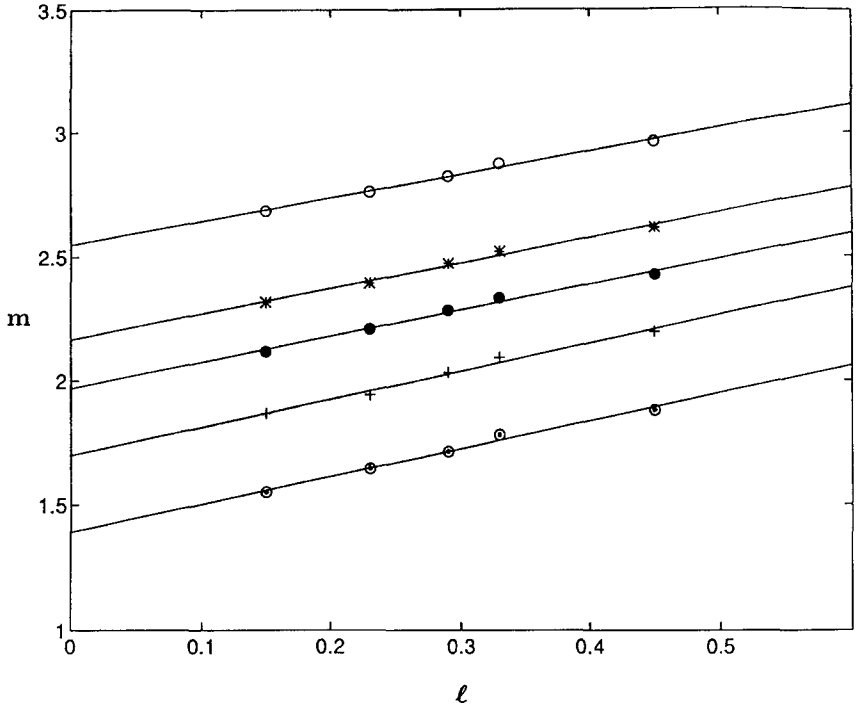

Fig. 6. The weight m of the aggregates remaining in the solution versus the molecular diameter ℓ. Symbols (the same as in Fig. 4) on each line represent the data at a fixed R for the various solvents.

aggregates remaining in the solution and m their weight, we have $m = \rho V$, or

$$m \sim \ell^{d_f[3+D_f(1-\tau)]/3} . \tag{10}$$

Eq. (10) tells us that a logarithmic plot of m versus ℓ should yield a straight line with a slope $p = d_f[3 + D_f(1 - \tau)]/3$. If the scattering results are to be believed, then $\tau = 2$, $d_f \simeq 2.5$ and $D_f \simeq 1.75$, and thus $p \simeq 1.04$. Direct measurement of ℓ is very difficult, and thus it can only be estimated roughly, or be related to another quantity that can be measured more easily. As already discussed above, the mean aggregate size $\langle s \rangle \sim M_s^z$. Indeed, heavier solvents with larger molecular diameters also generate larger aggregates. To show this, we present in Fig. 5 the MW distributions of the aggregates that are formed if n-C_5 and n-C_{10} are used as the solvents, and $R = 4$ (the details of the measurement of the MW distributions of these aggregates will be published elsewhere [25]). Fig. 5 provides two key clues to the molecular structure of the aggregates: (1) There are *two* maxima in the distributions, indicating the existence of *two* distinct types of structure, the DLA and DLCC aggregates, in agreement with our interpretation of the scattering data, and our proposal that one has to distinguish between the aggregates at small and large length scales. (2) The MW distribution with n-C_{10} is *broader*, indicating formation of larger aggregates, in agreement with what we find from the scaling analysis of the precipitation data. Thus we take ℓ to be

proportional to the characteristic diameter of the solvents. Fig. 6 shows the logarithmic plot of m versus ℓ. All the lines are parallel to one another, as they should be, since their slope depends only on the universal exponents τ, d_f, and D_f. We find $p \simeq 1.05$, in excellent agreement with the theoretical expectation $p \simeq 1.04$. Note that, only if we have two distinct fractal dimensions, d_f and D_f, does the predicted slope agree with that of the experiments, supporting again our contention that the structures of the small and large aggregates are different.

6. Discussions

We should point out that, instead of Eq. (2), a somewhat different equation for the total scattering intensity has also been proposed in the past which is given by [26]

$$I(q) = A^2 \int s^2 n_s S_s(q) ds \,, \tag{11}$$

where A is the scattering amplitude, and $S_s(q)$ is the intra-cluster structure factor given by

$$S_s(q) = \frac{\sin[(D_f - 1)\tan^{-1}(qR_s)]}{qR_s(D_f - 1)(1 + q^2R_s^2)^{(D_f-1)/2}} \,. \tag{12}$$

Here R_s is the radius of gyration of the fractal aggregate with s elementary particles in it, and thus $R_s \sim s^{1/D_f}$. Liu et al. [27] assumed that

$$n_s \sim s^{-\tau} \exp(-s/\langle s \rangle) \,, \tag{13}$$

and argued that, since $s = 1$ is the smallest aggregate size, n_s must be properly normalized. They then expressed the normalized n_s in terms of $\langle s \rangle$

$$n_s = \frac{\langle s \rangle^{\tau-2} s^{-\tau}}{\Gamma(2 - \tau, 1/s)} \exp(-s/\langle s \rangle) \,, \tag{14}$$

where $\Gamma(a, b)$ is the incomplete Gamma function. However, we should point out that Eq. (13) is more appropriate for equilibrium structures, such as percolation clusters [28–30], than for non-equilibrium aggregates, such as those considered here. In any event, assuming the validity of this equation for the non-equilibrium aggregates studied in this paper, one can substitute Eqs. (12) and (14) into (11) to finally obtain

$$I(q) = \frac{\langle s \rangle}{\Gamma(2 - \pi)} \left[F(3 - \tau, x)(1 + x^2)^{-D_f(3-\tau)/2} + G(2 - \tau, x) \left(\frac{x}{h} \right)^{-D_f} \right] \,, \tag{15}$$

in which $x = \xi q$, with ξ being some sort of a correlation length defined by

$$\xi \sim h \langle s \rangle^{1/D_f} \,. \tag{16}$$

Here $\Gamma(x)$ is the Gamma function, $F(a, x) = \Gamma(a) - \Gamma(a, u)$, with

$$u = \left[\frac{h^2(1 + x^2)}{x^2} \right]^{D_f/2} \,, \quad h = \left[\frac{D_f(D_f + 1)}{6} \right] \,, \tag{17}$$

and

$$G(a,x) = \sin\left[\frac{(D_f-1)\pi}{2}\right]\frac{\Gamma(a,y)}{D_f-1}, \tag{18}$$

with $y=(x/h)^{D_f}$. Thus, one can fit the scattering data to Eq. (15), treating D_f and τ as the adjustable parameters. Since τ takes on distinct values for each family of fractal structures, one can obtain insight into their structure by estimating τ. For example, for percolation $\tau \sim 2.18$, for DLCC aggregates $\tau = 2$, and for reaction-limited cluster–cluster aggregates [31] $\tau = 3/2$. Obviously, this procedure is much more elaborate than fitting the data to Eq. (4). It is particularly appropriate when the $I(q)$ versus q data do not show any clear trends. However, for the present problem this elaborate procedure yields results that are consistent with what we obtain from Eq. (4), and therefore we believe that our interpretation of the data is appropriate. For example, if we use Eq. (15) to fit the data of Fig. 1 at large length scale, we obtain $D_f \simeq 1.8 \pm 0.1$ and $\tau \simeq 1.9 \pm 0.1$, completely consistent with we obtained before.

Our results have important implications. First of all, they imply that the vast knowledge already available for aggregation processes can be applied immediately to the present problem. For example, an important problem is the molecular weight (MW) distribution of these aggregates and its evolution with time. To tackle this problem one can use the Smoluchowski equation to study the evolution of the aggregate-size distribution $n_s(t)$, and thus the MW distribution which is directly related to $n_s(t)$ [25,32]. This will also allow one to place an upper bound on the MW of the aggregates, which is also an unsolved problem. Secondly, one may predict [33] the *onset* of precipitation of the aggregates on the pore surfaces of the porous medium, and thus in a practical situation avoid this point to prevent any damage to the medium by the precipitation. These issues will be discussed elsewhere.

Acknowledgements

Partial support of this work by the Department of Energy is gratefully acknowledged. We would like to thank Professor Bahram Dabir for many useful discussions.

References

[1] M. Sahimi, G.R. Gavalas and T.T. Tsotsis, Chem. Eng. Sci. 45 (1990) 1443.
[2] M. Sahimi and A.O. Imdakm, Phys. Rev. Lett. 66 (1991) 1169.
[3] A.O. Imdakm and M. Sahimi, Chem. Eng. Sci. 46 (1991) 1977.
[4] L.M. Schwartz, D.J. Wilkinson, M. Bolsteri and P. Hammond, Phys. Rev. B 47 (1993) 4953.
[5] M.Y. Corapcioglu, N.M. Aboud and A. Haridas, in: Advances in Transport Phenomena in Porous Media, NATO Advanced Studies Institutes, Ser. E, No. 128 (Plenum, New York, 1987).
[6] H. Soo. and C.J. Radke, AIChE J. 31 (1985) 1926.
[7] V.N. Burganos, C.A. Paraskeva and A.C. Payatakes, AIChE J. 41 (1995) 272.
[8] R.L. Nortz, R.E. Baltus and P. Rahimi, Ind. Eng. Chem. Res. 29 (1990) 1968.
[9] V.S. Ravi-Kumar, T.T. Tsotsis, M. Sahimi and I.A. Webster, Chem. Eng. Sci. 49 (1994) 5789.

[10] A. Hirchberg, L.N.J. de Jong, B.A. Schipper and J.G. Meijer, Soc. Pet. Eng. J. 24 (1984) 283.
[11] J.G. Speight, The Chemistry and Technology of Petroleum (Marcel Dekker, New York, 1991).
[12] K. Drake, J. Bauer, T. Serafini and P. Cheng, eds., Proc. 39th International SAMPE Symp. (Society for Advanced Materials and Process Engineering, Anaheim, CA, 1994).
[13] M. Sahimi, Flow and Transport in Porous Media and Fractured Rock (VCH, Weinheim, Germany, 1995).
[14] H. Toulhoat, C. Prayer and G. Rouquet, Colloids Surf. 91 (1994) 267.
[15] T.A. Witten. and L.M. Sander, Phys. Rev. Lett. 47 (1981) 1400.
[16] P. Meakin, Phys. Rev. Lett. 51 (1983) 1119.
[17] M. Kolb, R. Botet and R. Jullien, Phys. Rev. Lett. 51 (1983) 1123.
[18] E. Bouchaud, M. Delsanti, M. Adam, M. Daoud and M. Durand, J. Physique 47 (1986) 1273.
[19] T. Vicsek and F. Family, Phys. Rev. Lett. 52 (1984) 1669.
[20] E.Y. Sheu, K.S. Liang, S.K. Sinha and R.E. Overfield., J. Colloid Interface Sci. 153 (1992) 399.
[21] P. Meakin, J. Chem. Phys. 81 (1984) 4637.
[22] C.W. Dwinggins, J. Apply. Cryst. 11 (1978) 615.
[23] N.F. Carnahan et al., Langmuir 9 (1993) 2035.
[24] Y. Kantor and T.A. Witten, J. Phys. Lett. 45 (1984) L675.
[25] B. Dabir, M. Nematy, A.R. Mehrabi, H. Rassamdana and M. Sahimi, Fuel 75 (1996) 1633.
[26] S.H. Chen and J. Teixeira, Phys. Rev. Lett. 57 (1985) 2583.
[27] Y.C. Liu, E.Y. Sheu, S.H. Chen and D.A. Storm, Fuel 74 (1995) 1352.
[28] D. Stauffer and A. Aharony, Introduction to Percolation Theory (Taylor and Francis, London, 2nd ed., 1994).
[29] M. Sahimi, Applications of Percolation Theory (Taylor and Francis, London, 1994).
[30] A. Bunde and S. Havlin, Fractals and Disordered Systems (Springer, Berlin, 1992).
[31] R.C. Ball, D.A. Weitz, T.A. Witten and F. Leyvraz, Phys. Rev. Lett. 58 (1987) 274.
[32] H. Rassamdana and M. Sahimi, AIChE J. 42 (1996) 3318.
[33] H. Rassamdana, B. Dabir, M. Nematy, M. Farhani and M. Sahimi, AIChE J. 42 (1996) 10.